Croatian Society for Materials Protection

*Metalurgija/Metallurgy*

**Vol. 65 No 1 / 2026**

# Influence of Residual Temperature on Microstructure Evaluation of Cast-Rolled 6061 Sheet

https://doi.org/10.64486/m.65.1.1

**Wen-lin Gao[1,2,3,4,*], Wei Chen[6], Rui-jue Wang[2], Ji-cheng Wang[2], Feng Sun[2], Cheng-ning Lie[5]**

[1] AECC Beijing Institute of Aeronautical Materials, Beijing 100095, China; gwl1504@126.com
[2] Hexing Aeronautical Materials (Tianjin) Technology Co., Ltd., Tianjin 300399, China; wrj5161@126.com; wjc5413@126.com; sf541863@163.com
[3] Beijing Engineering Research Center of Advanced Aluminum Alloys and Applications, Beijing 100095, China
[4] Advanced Aluminum Alloy Technology Innovation Center, Beijing 100095, China
[5] School of Materials Science and Engineering, Tianjin University, Tianjin, 300350, China; li515123@163.com
[6] School of Material and Metallurgy, University of Science and Technology Liaoning, Anshan 114051, China; ustl_wang@163.com
* Correspondence: gwl1504@126.com

***Type of the Paper:*** Article
***Received:*** May 20, 2025
***Accepted:*** August 6, 2025

**Abstract:** In this paper, a rolling process at residual temperatures is proposed. Special attention is given to the effects of different process parameters (e.g., residual rolling temperature and residual strain rate) on the microstructural evolution of cast-rolled 6061 aluminum alloy sheet. It was found that excellent grain refinement and a uniform structure (i.e., an average shrinkage cavity size of 13.71 μm and minimal grain size) were achieved at a residual rolling temperature of 390 ℃. With increasing rolling reduction, the grains in the core became more refined, and the grain size difference between the surface and central layers was reduced. Furthermore, the α(AlFeSi) phase was fragmented and dispersed with increasing pressure.

**Keywords:** residual temperature rolling; process parameters; structure property

## 1. Introduction

Twin-roll casting and rolling are among the leading processes in forming technologies. Under the cooling and rolling action of the casting roll, the molten metal initially undergoes two stages: solidification and plastic deformation. The metal is then rolled out from the roll gap in the form of a thin strip. Twin-roll casting and rolling can substitute the traditional casting, sawing and other similar technologies that are usually required to produce aluminum sheets with a short production cycle. Fabricating aluminum alloy sheets through twin-roll casting and rolling has become a significant manufacturing process in the aluminum industry, both nationally and internationally, owing to its advantages such as a simplified production process, low energy consumption and shorter production cycle [1-5]. However, twin-roll casting and rolling processes suffer from challenges such as poor formability and uneven grain structure distribution (metal material segregation) [6-9].

According to Huaping [10], when the shear force generated by the deformation during casting and rolling exceeds the shear strength of the solidified metal, micro-cracks can form at the edge and within the core of the cast-rolled sheet. If the micro-cracks are not controlled, they will develop into macro-cracks at the edge of the sheet. Wei [11] established that during the solidification of aluminum alloy in the molten pool, the solute content of the liquid phase gradually increases with the advancement of the solidification interface. This eventually



https://doi.org/10.64486/m.65.1.1

leads to the uneven distribution of elements in each part of the casting macro-scale to form macro-segregation, hence reducing the physical and mechanical properties of the material. Currently, the methods aimed at preventing the defects in aluminum alloy casts and rolled sheets mainly include trace element doping [12], electromagnetic stirring [13], residual temperature rolling [14], etc. Among them, adding the trace elements to the alloy is a relatively easy way to form the segregation during the solidification process, making the composition of the sheet non-uniform. In turn, electromagnetic stirring is an expensive technique with limitations. For instance, the process parameters are highly sensitive and require precise matching of frequency and current. Moreover, under conditions of high-speed casting and rolling, the effectiveness of electromagnetic stirring may diminish due to the reduced melt residence time, thereby necessitating dynamic adjustments of the parameters and increasing the difficulty of operation.

Some researchers have found that the residual heat remaining in the cast-rolled sheet immediately after production can be utilized for secondary rolling, enhancing efficiency. Various experiments also demonstrate that the residual rolling temperature is advantageous in terms of cost efficiency and plays a significant role in refining the grain structure and improving the comprehensive performance of the product. Zhang [14] reported that warm rolling can substantially improve the microstructure and mechanical properties of the sheet. Similarly, Yu [15], Satish [16] and Naronikar [17] concluded that a suitable residual temperature during rolling can greatly enhance the microstructure and comprehensive properties of cast and rolled sheets.

The application of light pressure deformation is an important method for improving plate properties. Among the existing rolling processing methods, low-temperature rolling produces ultra-fine grains, improves surface quality, reduces energy consumption, and increases productivity, making it highly suitable for current industrial processes. However, materials processed at low rolling temperatures typically exhibit poor ductility. In light of this, the present study aims to investigate the effects of different process parameters (e.g., residual rolling temperature and residual temperature-rolling reduction ratio) on 6061 aluminum alloy cast-rolling sheets. The mechanisms of action of those parameters were described based on numerical simulations, and the post-temperature rolling process was afterward designed to obtain high-performance 6061 cast-rolled sheets with the minimum strength and good plasticity. At the same time, the structural evolution law of materials in the post-temperature rolling stage was explored to find the method of regulating structural defects in 6061 cast and rolled sheets.

## 2. Materials and Methods

The 6061 aluminum alloy was produced using a medium-frequency induction melting furnace with a graphite-clay crucible. Once the temperature was reduced to 695 °C, an NF6-300 vertical twin-roll strip continuous casting machine was employed for casting and rolling. The casting and rolling parameters included a pouring temperature of 690 °C, a roll gap of 3 mm, and a casting-rolling speed of 12 m/min. The twin-roll casting and rolling were performed until a slab with a thickness of about 3.5 mm was obtained. The casting and rolling experimental parameters of the relevant cast-rolled plates are listed in Table 1. After air cooling, the metal was transported to the vertical rolling mill for the one-time residual temperature rolling. The process parameters of residual heat rolling are given in Table 2. The chemical composition of the alloy is summarized in Table 3.

Table 1. Experimental process parameters of 6061 aluminum alloy cast-rolled strip

| Technology | Technological Parameter |
|---|---|
| Melting temperature / ℃ | 720~750 |
| Casting temperature / ℃ | 670~710 |
| Casting and rolling speed / m·s-1 | 12~14 |
| Reserve the roller gap / mm | 2~5 |
| Height of the molten pool / mm | 170 |


https://doi.org/10.64486/m.65.1.1

**Table 2.** Process parameters of residual temperature rolling

| Residual heat rolling temperature / ℃ | Thickness before rolling mm | Thickness after rolling mm | Deformation rate % |
|---|---|---|---|
| 300 | 3.500 | 3.150 | 10 |
| 330 | 3.500 | 3.150 | 10 |
| 360 | 3.500 | 2.975 | 15 |
| 360 | 3.500 | 2.800 | 20 |
| 360 | 3.500 | 2.625 | 25 |
| 360 | 3.500 | 2.450 | 30 |
| 390 | 3.500 | 3.150 | 10 |

**Table 3.** Chemical composition of alloys / wt.%

| Alloy | Si | Mg | Fe | Mn | Cu | Cr | Ti | Zn |
|---|---|---|---|---|---|---|---|---|
| 6061 | 0.76 | 1.04 | 0.23 | 0.04 | 0.32 | 0.14 | 0.02 | 0.04 |

The finished plates produced by casting and rolling were cut into rectangular plates with dimensions of 250×100×3 mm using a shearing machine. Then, a wire cutting machine was employed to cut the plates into 12×10×3 mm samples. The sampling schematic diagram is depicted in Figure 1.

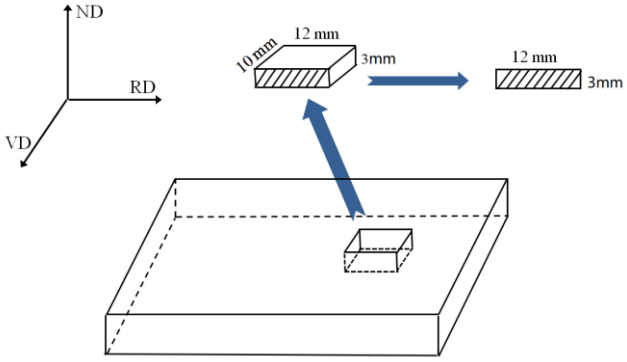


**Figure 1.** Sampling diagram

The samples were anodized after embedding and polishing to enhance the micro contrast. Subsequently, observations were made at 100x magnification using an electron microscope. The composition of the coating solution was 43 ml $H_3PO_4$ + 38 ml $H_2SO_4$ + 19 ml $H_2O$, the coating voltage was 25 V, and the coating time was 150 s. A Zeiss Axio Vert.A1 optical microscope was used to observe the microstructure along the rolling direction through the thickness of the plate. The obtained image was used to evaluate the grain shape, and the grain size was measured by means of the image-Pro Plus 6.0 software. The morphology and distribution of precipitated phases were monitored in the EVO MA 10 scanning electron microscope. The Vickers hardness tester was used to assess the hardness along the thickness direction under the experimental load of 100 g applied for 10 s. To ensure the accuracy of the experiment, the tests were performed at 10 random points on each sample. The highest and lowest points were then removed, and the average of the remaining 8 points was taken as the final result. The hardness was also measured 3 times for each set of samples to count the standard deviation.

## 3. Results and discussion

Figure 2 depicts the cast-rolled 6061 aluminum alloy sheet along the cross-section direction at the edge, the transition zone, and the core after anode coating with the rolling reduction rate of 20 % and the residual rolling temperatures of 300 ℃, 330 ℃, 360 ℃, and 390 ℃, respectively. At a residual rolling temperature of 300 ℃ (Figure 2a), the edge of the sheet exhibits a dense microstructure. Large shrinkage holes are observed in the center (Figure 2c) with an average size of 35.93 μm. When rolled at the residual temperature of 330 ℃, the


https://doi.org/10.64486/m.65.1.1

microstructure at the edge of the sheet (Figure 2d) is refined compared with that at 300 °C. In turn, the shrinkage hole in the center of the sheet (Figure 2f) is much smaller, possessing an average size of 27.91 μm. However, micro voids appeared on the edge of the sheet. This is because during the solidification process, the overlapping dendrites divided the melt, which then solidified and contracted. If these contracted regions are not replenished by subsequent melts, the irregularly shaped microscopic pores will be formed due to solidification and contraction, which is known as porosity. When the melt in the area solidifies, no other melt is added to form a loose structure. The shrinkage cavity in the core (Figure 2i) is noticeably bridged at a residual rolling temperature of 360 °C. The grain size difference between the edge (Figure 2g) and the core (Figure 2i) is also considerably reduced at this temperature. The residual rolling temperature exerts a clear refining effect on the core. This demonstrates that the sheet has a strong dynamic recovery at this temperature. As soon as the temperature rises to 390 °C, the average size of the shrinkage holes increases to 13.71 μm during the residual temperature rolling, and a uniform change is observed in the structure.

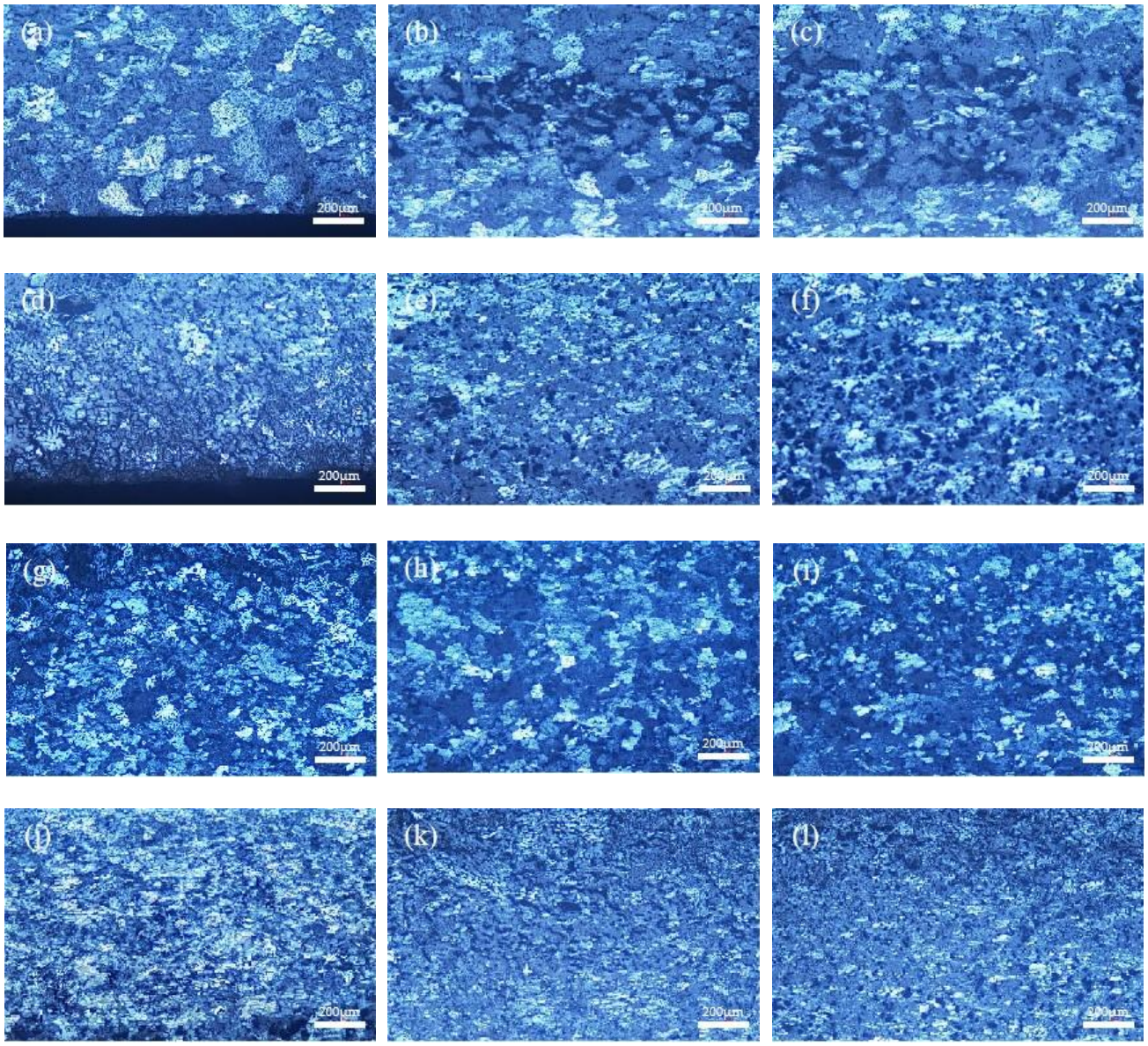


**Figure 2.** Cast-rolled 6061 sheets at different rolling temperatures (anodic coating)

Edge: (a) 300 °C; (d) 330 °C; (g) 360 °C; (j) 390 °C

Transition zone: (b) 300 °C; (e) 330 °C; (h) 360 °C; (k) 390 °C

Core: (c) 300 °C; (f) 330 °C; (i) 360 °C; (l) 390 °C


https://doi.org/10.64486/m.65.1.1

Figure 3 displays the grain size variations at the core and edge of cast-rolled 6061 plates, which are caused by different residual rolling temperatures. The graph reveals that the grain size increases with rising temperature. For the core, the lower residual temperature means that the longer air-cooling time is beneficial for the core grain growth. The grain size decreases gradually with the increase of rolling temperature. When the microstructure of the core is cast and rolled at 390 °C, the microstructure refinement effect is remarkable. This is due to the face-centered cubic structure of aluminum, which slips at high temperatures not only along the (111) planes but also along the (100) planes, thereby reducing the stacking fault energy and promoting dynamic recrystallization while healing damage and defects caused by plastic deformation. The high-temperature part of the center is equivalent to hot rolling, significantly improving the plasticity [18,19]. The overall grain size of the edge is greater than that of the core, which is due to the casting process.

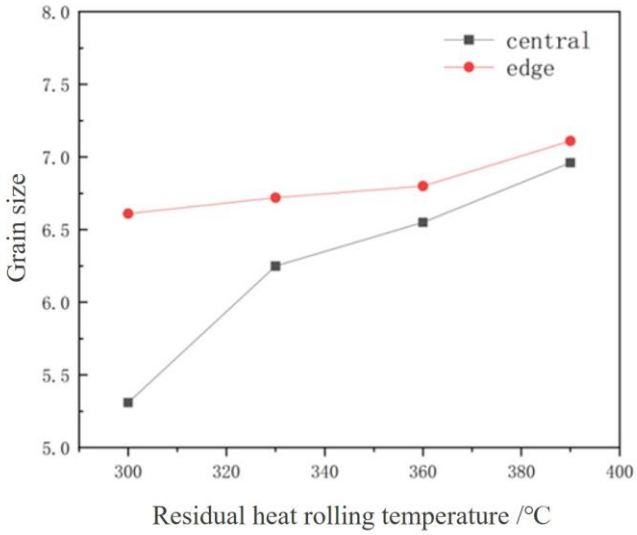


**Figure 3.** Variation in grain size with residual rolling temperature

Figure 4 shows the microstructure of the core region of cast-rolled 6061 aluminum alloy sheets subjected to rolling reductions of 5 %, 10 %, 15 %, 20 %, 25 %, and 30 % at a residual rolling temperature of 360 °C. As seen in the figure, the largest grain size appears in the sheet core and exhibits a relatively regular equiaxed crystal structure. Although the core exhibits a coarse grain structure, there is no obvious porosity, indicating that the temperature is appropriate. With the increase in pressure, the grains of the core are noticeably refined, and the recrystallization phenomenon becomes more pronounced.

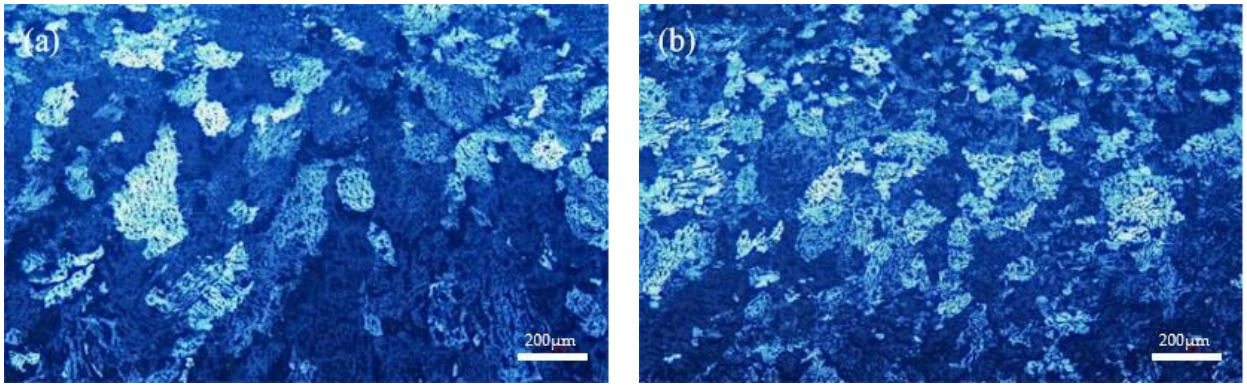



https://doi.org/10.64486/m.65.1.1

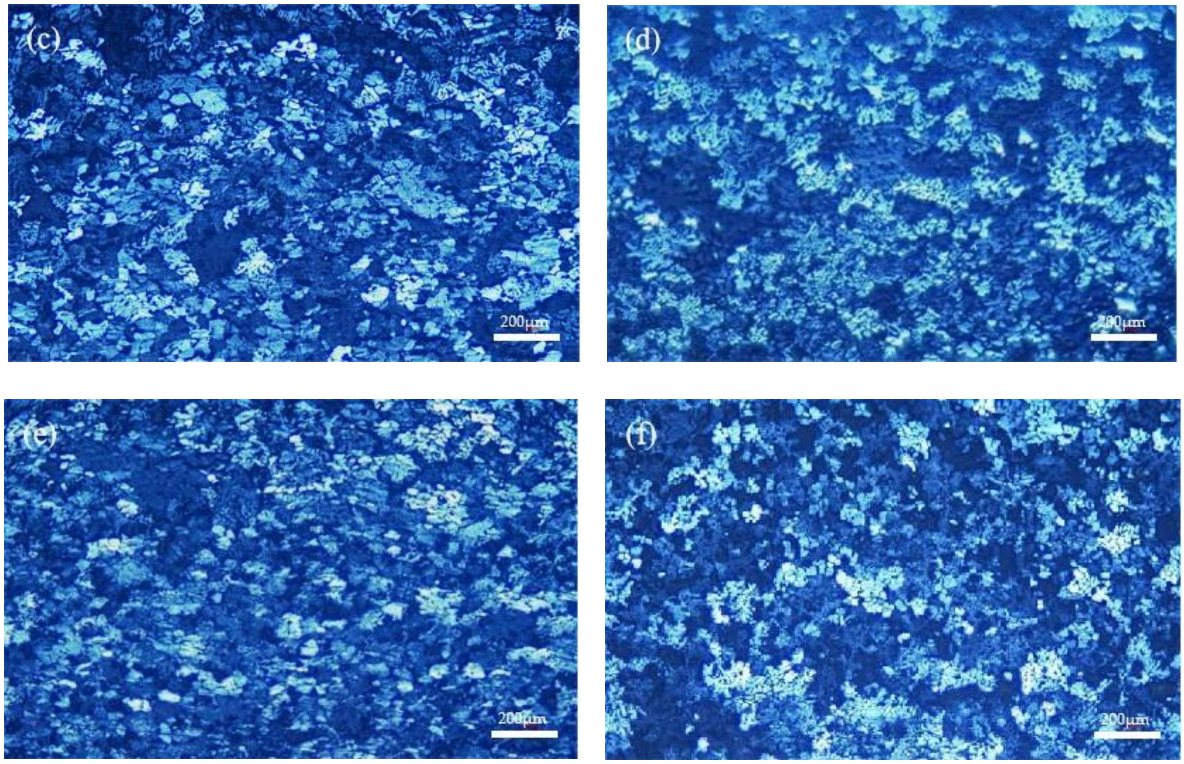


**Figure 4.** 6061 sheets after cast-rolling at different reduction rate (anodic coating)
(a) 5 %; (b) 10 %; (c) 15 %; (d) 20 %; (e) 25 %; (f) 30 %

Figure 5 depicts the grain size curve of the center of the sheet under different stress rates. As seen from the diagram, the grain size of the core shows an upward trend with the increase of reduction rate. The most obvious grain refinement is observed at a reduction rate of 15 %. With a further increase in the reduction rate, the grain growth gradually slows down, and the maximum grain size is attained at the reduction rate of 30 %. Increasing the rolling deformation can enhance the density of the composite material. With the increase in deformation, the amount of recrystallization also increases. The highest level of recrystallization is achieved at the deformation of 30 %. The second phase breaks and disperses as the reduction rate increases. Therefore, increasing the reduction rate to enhance the grain size and thereby improving the performance of the sheet is a very expedient solution.

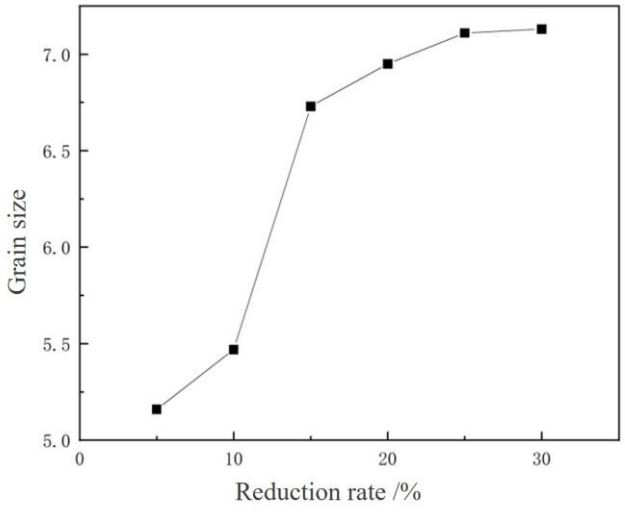


**Figure 5.** The influence of residual reduction rate on the grain size of the core of the plate


https://doi.org/10.64486/m.65.1.1

Figure 6 shows the SEM images of the core of cast-rolled 6061 aluminum alloy sheets at residual rolling temperatures ranging from 300 °C to 390 °C. At the residual rolling temperature of 300 °C (Figure 6a), the second phase in the core exhibits a network-like morphology. Combined with the energy-dispersive spectroscopy (EDS) analysis of the atomic ratio and the report in the literature [20], the phase is determined as β-AlFeSi. The coarse phase precipitated at these grain boundaries will seriously affect the comprehensive properties of the alloy, split the grains, weaken the intergrain bonds, and reduce the plastic toughness of the sheet. A black, spherical $\alpha$-AlFeSi phase appeared at the edge of the network and a few positions in the middle of the sheet. The higher energy is achieved at the edge of the β phase, and the increase in the free energy of the system caused by the nucleation at the edge is smaller than that at other positions. Since the driving force for the nucleation is greater at the edge, it is easier to generate the $\alpha$ phase at the edge of the β phase. The $\alpha$ phase growth at the edge of the mesh is also more pronounced. This is because the β→$\alpha$ phase transition is diffusion-type, and the β phase is in contact with the $\alpha$ phase [21,22]. This provides a fast channel for the Fe diffusion with a higher Fe concentration gradient. At the residual rolling temperature of 360 °C (Figure 6e), the network structure is broken, and the $\alpha$ phase continues to develop into a nearly spherical shape whereby the phase transformation is completed. At the residual rolling temperature of 390 °C (Figure 6g), the β phase becomes very small as the $\alpha$ phase continuously absorbs Mn, Fe and Si in the Al matrix during the growth process. This results in a short solute diffusion. At this time, the β→$\alpha$ phase transition is affected by the diffusion, and the $\alpha$ phase decreases. There are white and bright short rod-like $Mg_2Si$ phase inclusions appearing together with the $\alpha$ phase.

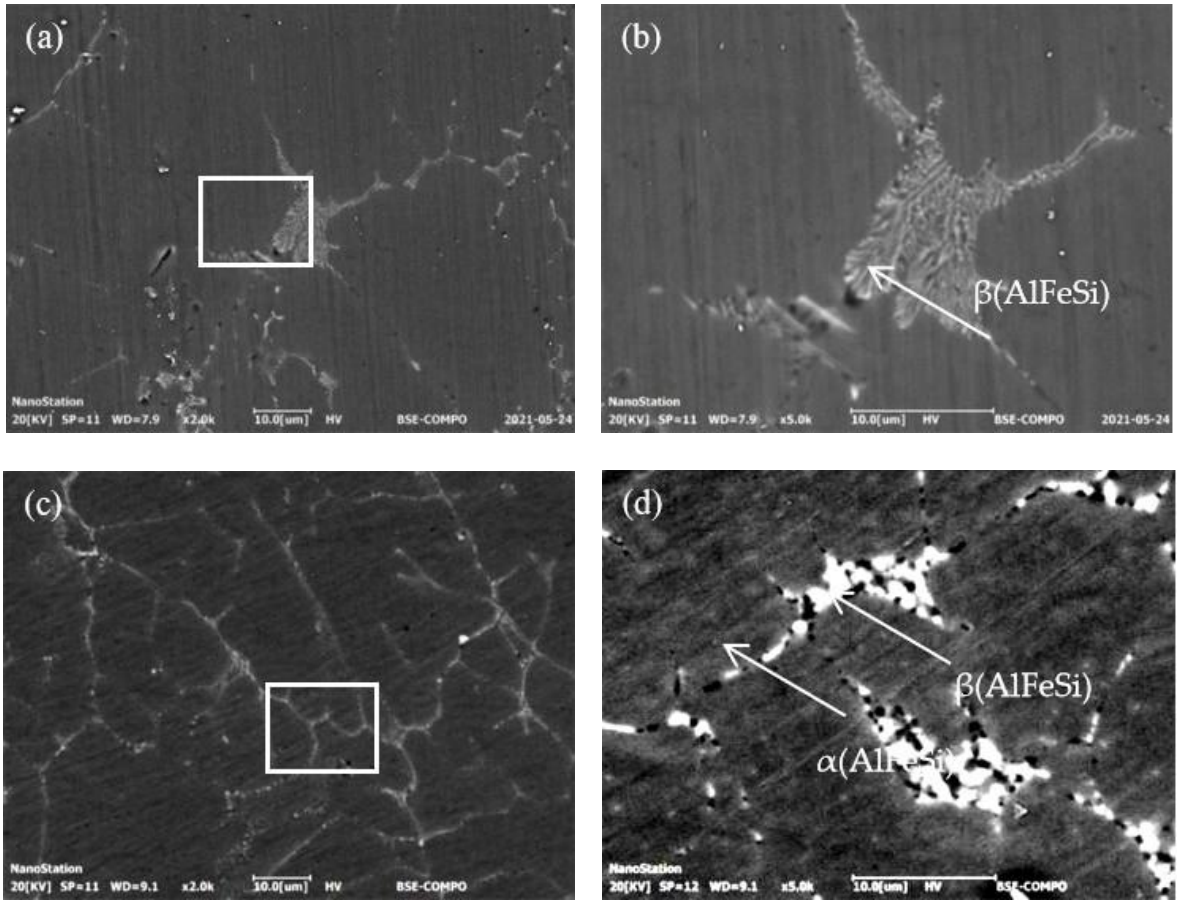



https://doi.org/10.64486/m.65.1.1

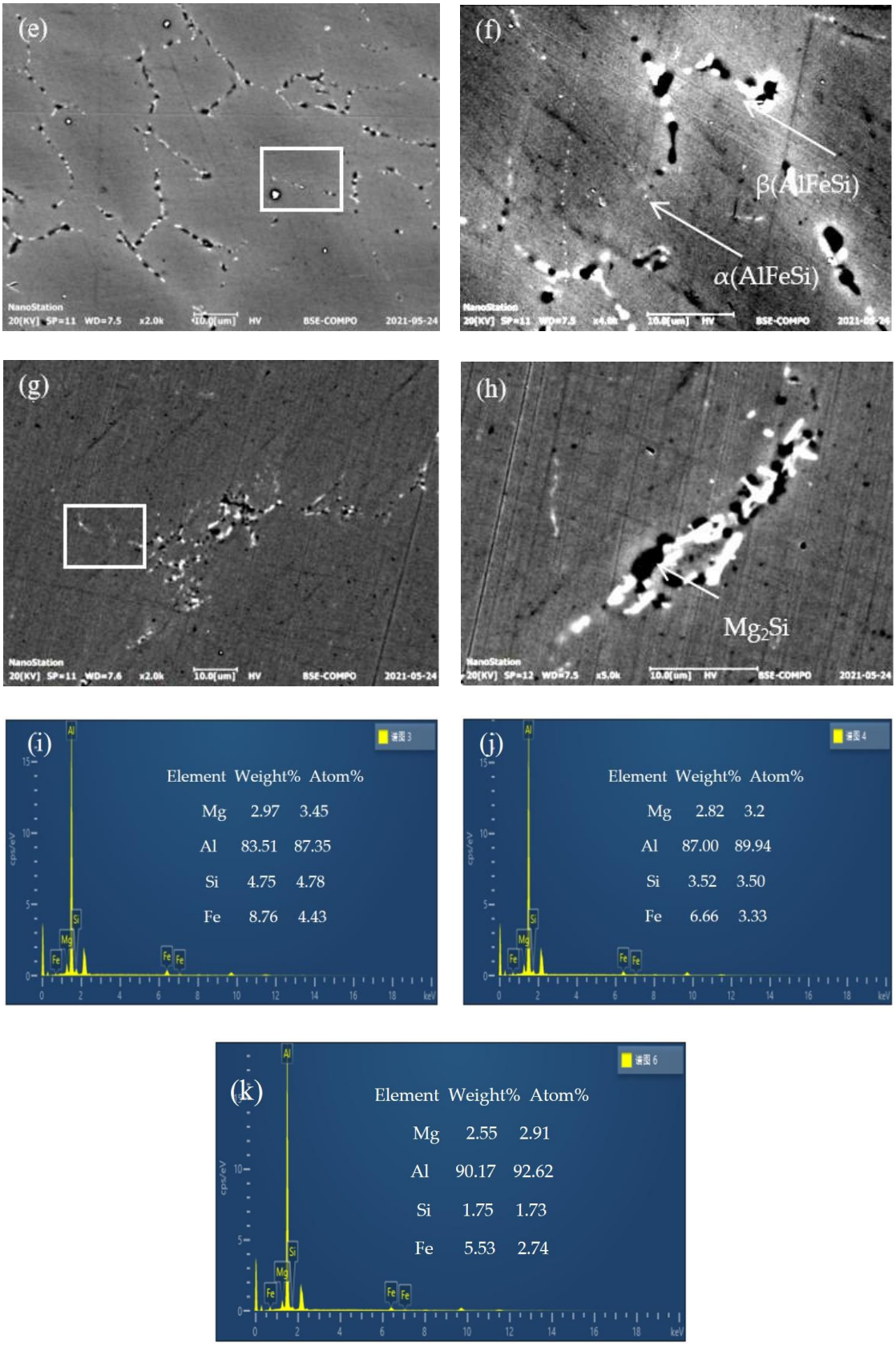


**Figure 6.** SEM and EDS images of cast-rolled 6061 sheets at different rolling temperatures
Low magnification: (a) 300 °C; (c) 330 °C; (e) 360 °C; (g) 390 °C; High magnification: (b) 300 °C; (d) 330 °C; (f) 360 °C; (h) 390 °C; (i) β-AlFeSi in (b); (g) *α*-AlFeSi in (f);(k) $Mg_2Si$ in (h)


https://doi.org/10.64486/m.65.1.1

Figure 7 shows SEM images of the cast-rolled 6061 sheet at different reduction rates. It can be observed that the deformation amount increases to 10 % (Figure 7b). Meanwhile, the thickness of the sheet after rolling is reduced to 3.15 mm, and the relatively brittle second-phase particles are broken. In cast-rolled 6061 aluminum sheets, the $\alpha$-AlFeSi phase is particularly prone to fragmentation. With the increase of the residual rolling deformation (Figures 7c-7f), the shape of the easily broken second-phase particles becomes more defined.

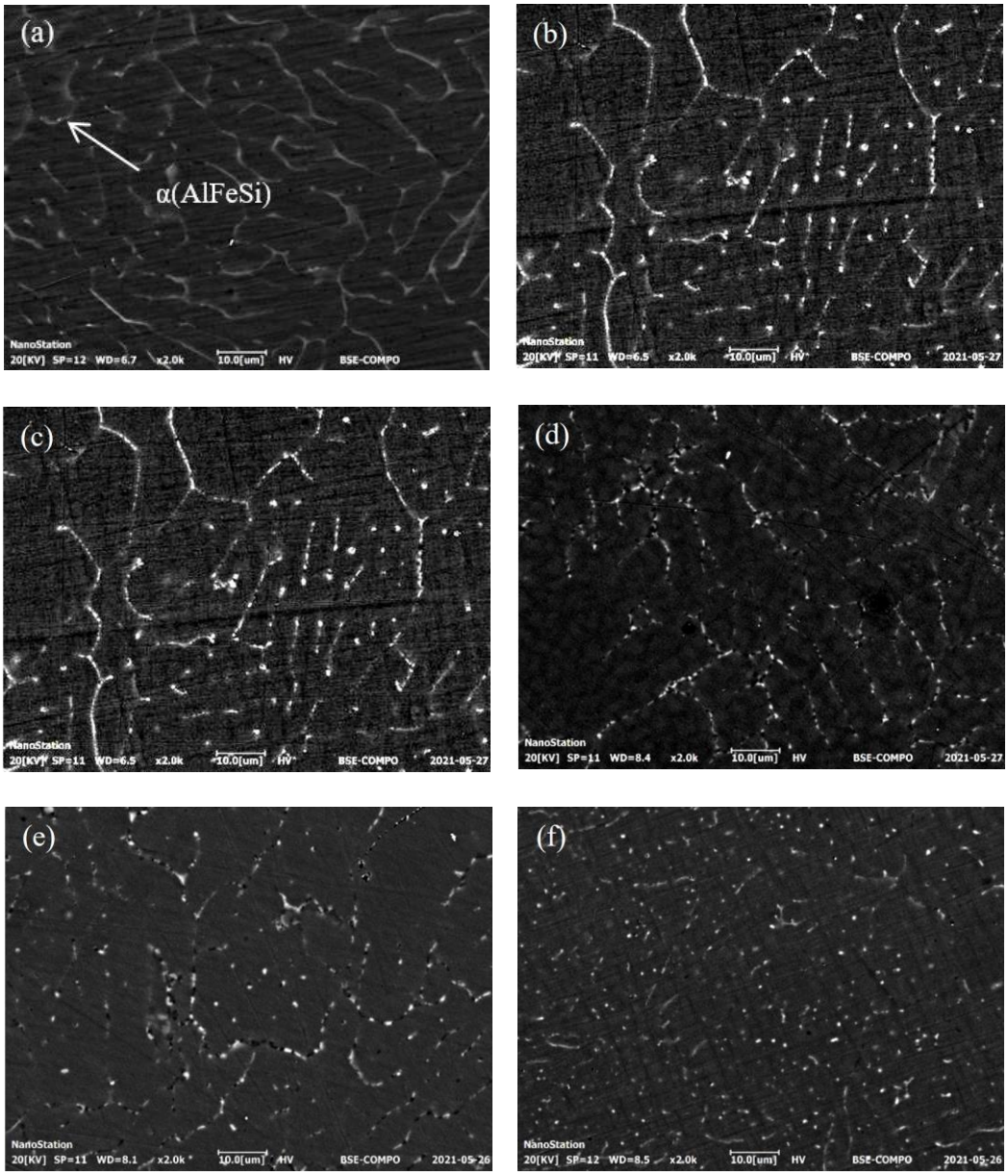


**Figure 7.** SEM images of cast-rolled 6061 sheets at different reduction rates
(a) 0 %; (b) 10 %; (c) 15 %; (d) 20 %; (e) 25 %; (f) 30 %

Figure 8 presents the microhardness profile of the plate at various residual rolling temperatures.

As shown in the figure, the highest core hardness of 76.98 HV0.1 is achieved at approximately 300 °C. This is because the dynamic precipitation time of the secondary Fe-rich phase in the core is long and sufficient at this temperature. With the increase in temperature to 330 °C, the $\beta \rightarrow \alpha$ phase transition occurs in the core, the shape changes from long strips to spherical shapes, and the hardness of the core decreases to 74.79 HV0.1. At


https://doi.org/10.64486/m.65.1.1

390 °C, the dynamic recrystallization arises. This is because the higher the temperature, the faster the recrystallization rate. Furthermore, the absence of an incubation period results in the formation of fine recrystallized grains, leading to strengthening of the material [23, 24]. Composed of short rod-like $Mg_2Si$ and $\alpha$ phases, the material exhibits an increase in hardness to 74.67 HV0.1. Moreover, the overall hardness of the edge at 330 °C (71.36 HV0.1) is less than that of the core by 5.62 HV0.1. Once the temperature increases to 360 °C, the minimum hardness difference between the core and the edge is 0.34 HV0.1. At this time, the residual rolling temperature greatly reduces the hardness difference caused by centerline segregation.

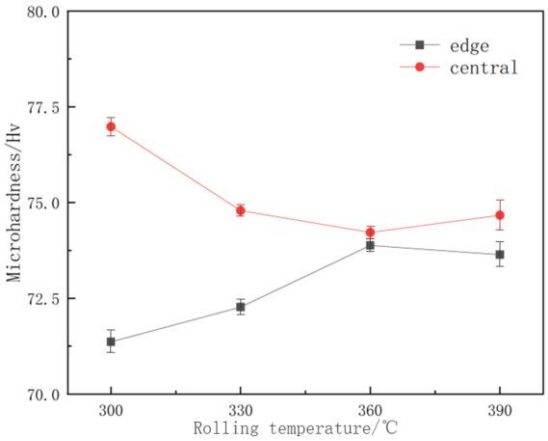


**Figure 8.** Micro-hardness curve of residual temperature rolled plate

Figure 9 illustrates the microhardness curves of plates with different reduction rates. The hardness values at both the central and edge regions initially decrease and then increase. The overall hardness of the center exceeds that of the edge, which is due to the high content of the second phase in the center and the large deformation concentration [25]. Without applied pressure (0 % reduction), the hardness of the core reaches 80.1 HV0.1. This is because the high-temperature core is more prone to deformation. With the increase in reduction rate to 10 %, the network second phase in the core is broken, and the hardness decreases to 75.23 HV0.1, whereas the reduction rate continues to increase. The dispersion of the second phase induces strengthening, and the hardness of the center of the cast-rolled plate begins to increase gradually. At the reduction rate of 30 %, the maximum hardness is 79.5 HV0.1. For the edge, as the reduction rate increases from 0 % to 15 %, the hardness changes to a small extent. Moreover, the second-phase particles in the central layer with the higher second-phase content also begin to gradually move toward the surface layer as the deformation proceeds. At the reduction rate above 20 %, the hardness of the edge shows an increasing trend.

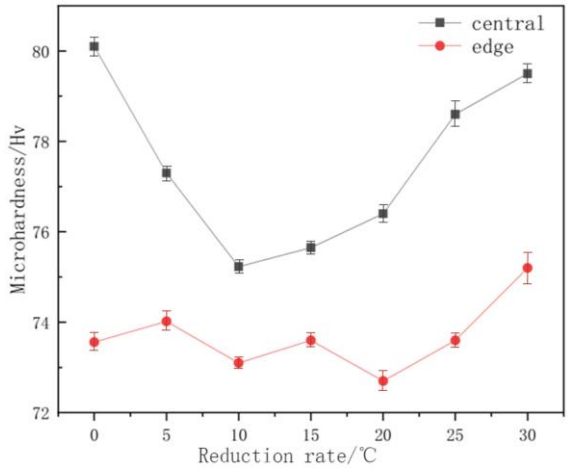


**Figure 9.** Microhardness curves of residual hot-rolled plates with different reduction rates


https://doi.org/10.64486/m.65.1.1

The temperature measurement instruments used in the test have an inherent measurement error of ± 3 ℃ Moreover, during the residual rolling process, factors such as heat transfer in the roller track and environmental heat dissipation may cause the actual temperature gradient between the surface and the core of the cast billet to exceed the predicted range of the model, thereby affecting the grain size and the second phase distribution. Although the temperature drop stability and the alloy composition uniformity were optimized by preheating the crucible to 300 ℃and holding it for a period of time after the 6061 aluminum alloy ingot was melted to ensure the complete dissolution of the alloy elements, temperature fluctuations at the microscopic scale might have still caused the uneven distribution of the plate composition and batch differences during the sample testing. It is worth noting that the above-mentioned limitations may introduce a ± 5 % prediction error in key performance indicators such as hardness and grain size. However, they do not significantly alter the qualitative conclusions of the study, particularly that increasing rolling deformation improves the density of the composite material. Future studies may improve accuracy by employing high-precision temperature control and multi-batch big data modeling approaches.

## 4. Conclusions

The rolling temperature has a significant effect on the phase change in the core of the sheet. At a residual rolling temperature of 300 ℃, the average diameter of the shrinkage holes in the core is 35.93 μm. In contrast, at 360 ℃, these cavities are nearly eliminated. The iron-rich reticulate β phase, which deteriorates mechanical performance, transforms into a spherical $\alpha$ phase. When the temperature reaches 390 ℃, the $Mg_2Si$ strengthening phase forms. At this stage, the residual rolling temperature is comparable to hot rolling conditions at the central region of the sheet. The rolling reduction significantly influences grain refinement in the cast-rolled 6061 sheet. Once the sheet is rolled at a residual temperature of 390 ℃, the grains in the core are refined. The grain size difference between the surface and the central layers is reduced, and the second-phase network is broken. The effect of the broken $\alpha$ phase on the rolling force is more dispersed with the increase of the reduction ratio. Therefore, in practical industrial applications, the grain size of cast-rolled 6061 plates can be increased by rolling and thickening, thereby improving the performance of the plates.

Meanwhile, several potential sources of uncertainty should be considered in the interpretation of our findings.

**Acknowledgments:** This work was financially supported by the National Natural Science Foundation of China (project no.52274391).

## References

[1] A. D. Efa, "Laser beam welding parametric optimization for AZ31B and 6061-T6 alloys: residual stress and temperature analysis using a CCD, GA and ANN," *Optics and Laser Technology*, vol. 175, art. no. 110837, 2024., https://doi.org/10.1016/j.optlastec.2024.110837

[2] K. Huang, P. Y. Yi, Q. S. Huang et al., "Effect of quenching cooling rate on residual stress and microstructure evolution of 6061 aluminum alloy," *Journal of Central South University*, vol. 31, no. 7, pp. 2167–2180, 2024., https://doi.org/10.1007/s11771-024-5705-5

[3] Y. Ding, J. Wang, M. Zhao *et al.*, "Effect of annealing temperature on joints of diffusion bonded Mg/Al alloys," *Transactions of Nonferrous Metals Society of China*, vol. 28, no. 2, pp. 251–258, 2018., https://doi.org/10.1016/j.matlet.2022.132491

[4] D. Kikuchi, Y. Harada and S. Kumai, "Surface quality and microstructure of Al–Mg alloy strips fabricated by vertical-type high-speed twin-roll casting," *Journal of Manufacturing Processes*, vol. 37, pp. 332–338, 2019., https://doi.org/10.1016/j.jmapro.2018.12.007


https://doi.org/10.64486/m.65.1.1

[5] A. G. Kumar, P. Satwik, P. Denis *et al.*, "Effects of heat treatment on the surface quality and improvement in formability of deformation-machined products of Al 6061," *Journal of Manufacturing Science and Engineering*, vol. 144, no. 12, 2022., https://doi.org/10.1115/1.4054991

[6] S. Das, N. Lim, J. Seol *et al.*, "Effect of the rolling speed on microstructural and mechanical properties of aluminum–magnesium alloys prepared by twin roll casting," *Materials & Design*, vol. 31, no. 3, pp. 1633–1638, 2010., https://doi.org/10.1016/j.matdes.2009.08.032

[7] M. Baek, K. Euh and K. Lee, "Microstructure, tensile and fatigue properties of high-strength Al 7075 alloy manufactured via twin-roll strip casting," *Journal of Materials Research and Technology*, vol. 9, no. 5, pp. 9941–9950, 2020. https://doi.org/10.1016/j.jmrt.2020.06.097

[8] Y. L., F. P. M. D. V., L. J. S. *et al.*, "Modeling of dynamic mode I crack growth in glass fiber-reinforced polymer composites: fracture energy and failure mechanism," *Engineering Fracture Mechanics*, early access, art. no. 107522, https://doi.org/10.1016/j.engfracmech.2020.107522

[9] S. Minghan, Z. Chuanxing, F. Shan *et al.*, "A novel design of electromagnetic side sealing in twin-roll strip cast-rolling process," *Mechanics Based Design of Structures and Machines*, vol. 49, no. 7, pp. 1–18, 2020., https://doi.org/10.1080/15397734.2019.1707687

[10] H. Tang, N. Li, C. Lei *et al.*, "Effect of hot deformation treatment on the microstructure and mechanical properties of selective laser melted AlSi10Mg alloy," *Materials Letters*, vol. 383, art. no. 137962, 2025., https://doi.org/10.1016/j.matlet.2024.137962

[11] H. Wei, J. Elmer and T. DebRoy, "Origin of grain orientation during solidification of an aluminum alloy," *Acta Materialia*, vol. 115, pp. 123–131, 2016., https://doi.org/10.1016/j.actamat.2016.05.057

[12] S.-Y. Chang, J.-Y. Lee, Y.-H. Huang, and A.-B. Wu, "Joining of AZ31 Magnesium Alloy to 6061 Aluminum Alloy with Sn-Zn Filler Metals Containing Trace Rare Earth Elements," *Applied Sciences*, vol. 9, no. 13, pp. 2655–2655, Jun. 2019., https://doi.org/10.3390/app9132655

[13] S. Wei, R. Zhang, X. Liu *et al.*, "Comparative study on the effect of external magnetic field on aluminum alloy 6061 and 7075 resistance spot-welding joints," *Metals*, vol. 14, no. 10, art. no. 1196, 2024., https://doi.org/10.3390/met14101196

[14] F. Z. Quan, Z. L. Yu, Z. L. Han *et al.*, "Experimental study on the twin-roll strip casting and warm rolling Fe-6.5 wt.% Si steel sheet," *Advanced Materials Research*, vol. 873, pp. 48–53, 2013., https://doi.org/10.4028/www.scientific.net/AMR.403-408.1274

[15] Y. Yu, K. Lin and P. Jiang, "Superplastic formability of AZ31 magnesium alloy sheets produced by twin roll casting and sequential hot rolling," *Modern Physics Letters B*, vol. 27, no. 19, art. no. 1341020, 2013., https://doi.org/10.4028/www.scientific.net/MSF.604-605.267

[16] R. D. Satish, R. D. Kumar and M. Merklein, "Effect of temperature and punch speed on forming limit strains of AA5182 alloy in warm forming and improvement in failure prediction in finite element analysis," *Journal of Strain Analysis for Engineering Design*, vol. 52, no. 4, pp. 258–273, 2017., https://doi.org/10.1177/0309324717704995

[17] H. A. Naronikar, A. H. Jamadagni, A. Simha *et al.*, "Optimizing the heat treatment parameters of Al-6061 required for better formability," *Materials Today: Proceedings*, vol. 5, no. 11, pp. 24240–24247, 2018., https://doi.org/10.1016/j.matpr.2018.10.219

[18] L. Zhang, Y. Wang, S. Ni *et al.*, "The evolution of second-phase particles in 6111 aluminum alloy processed by hot and cold rolling," *Journal of Materials Engineering and Performance*, vol. 27, no. 3, pp. 1130–1137, 2018., https://doi.org/10.1016/j.jmrt.2025.08.160

[19] S. Yu-chong, Z. Bing, X. Zhen *et al.*, "Microstructure evolution and recrystallization behavior of hot-rolled AA6061 twin-roll casting plate with different manganese contents," *Journal of Alloys and Compounds*, vol. 918, 2022., https://doi.org/10.1016/j.jallcom.2022.165618

[20] S. Shabestari, "The effect of iron and manganese on the formation of intermetallic compounds in aluminum–silicon alloys," *Materials Science & Engineering A*, vol. 383, no. 2, pp. 289–298, 2004., https://doi.org/10.1016/j.msea.2004.06.022

[21] G. Alistair, E. Ryan, Y. Yichao *et al.*, "Multiscale analysis of grain boundary microstructure in high-strength 7xxx Al alloys," *Acta Materialia*, vol. 202, pp. 190–210, 2021., https://doi.org/10.1016/j.actamat.2020.10.021

[22] T. Shuangyong, L. Su, X. Zhen *et al.*, "Study of the effect of Er on the homogenization of 6061 twin-roll casting sheet," *Journal of Materials Engineering and Performance*, vol. 32, no. 11, pp. 4911–4921, 2022., https://doi.org/10.1007/s11665-022-07441-9

[23] Z. Haixiao, S. Lu, Z. Guoqun *et al.*, "Abnormal grain growth behavior and mechanism of 6005A aluminum alloy extrusion profile," *Journal of Materials Science & Technology*, vol. 157, pp. 42–59, 2023., https://doi.org/10.1016/j.jmst.2023.02.013

[24] S. D. C. I., M. E. M., B. R. F. *et al.*, "Evidence for two-stage hardening in an Al-Zn-Mg-Cu alloy processed by high-pressure torsion," *Journal of Alloys and Compounds*, vol. 941, 2023., https://doi.org/10.1016/j.jallcom.2023.168839

[25] Z. Shao-You, W. Xuan, M. Yuan-Ting *et al.*, "Towards relieving center segregation in twin-roll cast Al–Mg–Si–Cu strips by controlling the thermal–mechanical process," *Journal of Materials Science & Technology*, vol. 148, pp. 31–40, 2023., https://doi.org/10.1016/j.jmst.2022.11.023


https://doi.org/10.64486/m.65.1.1